Power-spectrum-based neural-net connection admission control for multimedia networks

C.-J. Chang, L.-F. Lin, S.-Y. Lin and R.-G. Cheng

Abstract: Multimedia networks need sophisticated and real-time connection admission control (CAC) not only to guarantee the required quality of service (QoS) for existing calls but also to enhance utilisation of systems. The power spectral density (PSD) of the input process contains correlation and burstiness characteristics of input traffic and possesses the additive property. Neural networks have been widely employed to deal with the traffic control problems in high-speed networks because of their self-learning capability. The authors propose a power-spectrum-based neural-net connection admission control (PNCAC) for multimedia networks. A decision hyperplane is constructed for the CAC using power spectrum parameters of traffic sources of connections, under the constraint of the QoS requirement. Simulation results show that the PNCAC method provides system utilisation and robustness superior to the conventional equivalent capacity CAC scheme and Hiramatsu's neural network CAC scheme, while meeting the QoS requirement.

1 Introduction

Multimedia networks should be equipped with a set of traffic control functions to ensure the QoS of each service connection and to enhance system utilisation. One of the traffic control functions is connection admission control. Connection admission control (CAC) is defined as 'a set of actions taken by the network to determine whether a connection can be accepted' [1]. A new connection is accepted only if sufficient network resources are available and the required performance can be maintained.

Several conventional CAC control techniques for high-speed networks have been proposed. In the peak rate allocation, QoS is always guaranteed if the aggregate bit rate never exceeds the system capacity. However, it leads to low utilisation of network resources. An equivalent capacity (effective bandwidth) method was proposed to estimate the required bandwidth for individual or aggregate connections with desired QoS [2, 3]. A call admission scheme by inferring the upper bound of cell loss probability from the traffic parameters specified by users was studied in [4]. Also a simple bandwidth assignment policy by classifying all traffic sources was presented. All the studies were conducted mainly on the basis of traffic parameters in the time domain.

However, Li and Hwang [5] and Sheng and Li [6] have studied the queueing performance of a high-speed network from the point of view of frequency-domain traffic parameters. The process of input traffic inherently contains a power spectral density (PSD) function, which is the Fourier transform of the input traffic process's autocorrelation function. From their studies, two characteristics of PSD are demonstrated: (i) the PSD can be represented by three main parameters such as the DC component, the average power and the half-power bandwidth; and (ii) the low-frequency band of the input PSD has a dominant impact on queueing performance, while the high-frequency band can be neglected to a large extent.

This is because the low-frequency component of the PSD contains the correlation and burstiness of the input process. With more low-frequency components, the burstier the input traffic will be [7].

We have proposed a composition algorithm to obtain three new PSD parameters of a traffic source which is aggregated from two traffic sources in [8]. It can be concluded that PSD parameters possess the additive property; this makes the PSD parameters more suitable for admission control, no matter how many types of traffic sources there are. A power-spectrum-based table-lookup CAC method for multimedia communications in ATM networks was studied, where the table content was the cell loss probability indexed by PSD parameters of voice/video calls and arrival rates of data calls [8]. Simulation results revealed that it could achieve system utilisation 9% higher than that of the conventional equivalent capacity CAC method proposed in [2].

In recent years, neural networks have been widely employed to deal with the traffic control problems in high-speed multimedia networks [9–11]. A major feature of the neural network is the self-learning capability which can be utilised to characterise the relationship between input traffic and system performance. In [9], Hiramatsu proposed a connection admission controller using a neural network. Hiramatsu's neural network connection admission controller used the offered traffic characteristics and QoS requirement to decide whether to accept or reject a new call. Results showed that the neural network learned a complicated boundary for call acceptance decision. We previously proposed a neural network connection admission control (NNCAC) scheme [10] and a neural fuzzy connection admission control (NFCAC) scheme [11] for ATM networks. Simulation results reveal that call admission control with either neural networks or neural fuzzy

IEE Proceedings online no. 20020031

DOI: 10.1049/ip-com:20020031

Paper first received 13th November 2000 and in revised form 18th September 2001

The authors are with the Department of Communication Engineering, National Chiao Tung University, Hsinchu 300, Taiwan, Republic of China

networks can improve significantly the system utilisation under QoS constraint.

In this paper, we propose a power-spectrum-based neural-net connection admission control (PNCAC) method for multimedia networks. We first transform the time-domain parameters of source traffic of connections into the power-spectrum parameters in the frequency domain, then a decision hyperplane of the connection admission control is constructed under the constraint of QoS after the neural network has been trained. The decision hyperplane splits the sample space into two parts: one is for 'accept' and the other is for 'reject'. We further adopt the learning/adapting capabilities of the neural network to adjust the optimal location of the boundary between these two decision spaces (i.e. using the back-propagation training algorithm to adjust the link weights of PNCAC to the optimum value). Simulation results show that PNCAC achieves higher system utilisation, superior by 23.8% to the conventional equivalent capacity CAC proposed in [2], and comparable to that of Hiramatsu's neural network CAC (NNCAC) [9]. However, PNCAC is more robust than Hiramatsu's NNCAC in high-speed multimedia networks. As characteristics of traffic sources change, the connection number of each traffic type utilised as the input variables in Hiramatsu's NNCAC can no longer characterise the traffic. At this time, Hiramatsu's NNCAC should perform online training and even the node-growing or node-pruning learning process to adapt to the variation in traffic sources, otherwise, the performance would deeply degrade with the QoS no longer guaranteed. However, the proposed PNCAC can still perform well without any other modifications or retraining process.

2 Power spectrum of the input process

If an input rate process $a(t)$ is modelled as an $(M+1)$-state Markov-modulated Poisson process (MMPP), the MMPP can be represented by $(\boldsymbol{Q}, \boldsymbol{r})$, where $\boldsymbol{Q}$ is the state transition-rate matrix and $\boldsymbol{r}=[\gamma_0, \gamma_1, \ldots, \gamma_M]$ is the vector representing the arrival rate at each MMPP state. The stationary probability vector of state, denoted by $\boldsymbol{\Pi}=[\pi_0, \pi_1, \ldots, \pi_M]$, can be obtained by solving equations of $\boldsymbol{\Pi Q}=0$ and $\boldsymbol{\Pi e}=1$, where $\boldsymbol{e}$ is an unit column vector. The average input rate $\bar{\gamma}$ is then given by

$$\bar{\gamma} = \sum_{i=0}^{M} \gamma_i \pi_i \tag{1}$$

$\boldsymbol{Q}$ is diagonalisable and can be represented by spectral decomposition as

$$\boldsymbol{Q} = \sum_{l=0}^{M} \lambda_l \boldsymbol{g}_l \boldsymbol{h}_l \tag{2}$$

where λ_l is the lth eigenvalue of $\boldsymbol{Q}$, and $\boldsymbol{g}_l$ and $\boldsymbol{h}_l$ are the associated right column and left row eigenvectors of $\boldsymbol{Q}$ with respect to λ_l, respectively [6].

Then the autocorrelation function of the MMPP, defined as $R(\tau) \equiv \overline{a(t)a(t+\tau)}$, can be derived. Its corresponding PSD, denoted by $P(\omega)$, can also be given, via Fourier transformation of $R(\tau)$, by [6]

$$P(\omega) = \bar{\gamma} + 2\pi\Psi_0\delta(\omega) + \sum_{l=1}^{M} b_l(\omega) \tag{3}$$

where

$$\delta(\omega) = \begin{cases} \infty & \text{for } \omega = 0 \\ 0 & \text{elsewhere} \end{cases} \tag{4}$$

Ψ_0 is the DC component, given by

$$\Psi_0 = \bar{\gamma}^2 \tag{5}$$

and $b_l(\omega)$ is the bell-shaped function with respect to nonzero λ_l, given by

$$b_l(\omega) = \frac{\Psi_l B_l}{(B_l/2)^2 + (\omega - \omega_l)^2} \tag{6}$$

Ψ_l in (6) is the average power contributed by λ_l, given by

$$\Psi_l = \sum_i \sum_j \pi_i \gamma_i \gamma_j g_{li} h_{lj} \quad \text{for } 1 \le l \le M \tag{7}$$

where g_{li} and h_{lj} are the ith and jth entities of the vector $\boldsymbol{g}_l$ and $\boldsymbol{h}_l$, respectively. B_l in (6) is the half-power bandwidth, $B_l = -2Re\{\lambda_l\}$ and the ω_l in (6) is the central frequency of the bell-shaped function $b_l(\omega)$, $\omega_l = Im\{\lambda_l\}$, where $Re\{\cdot\}$ and $Im\{\cdot\}$ denote the real part and the imaginary part of the argument, respectively.

From (3), it can be found that the PSD of an MMPP process is constituted by white noise $\bar{\gamma}$, DC component $2\pi\Psi_0$, and a set of bell-shaped functions $b_l(\omega)$ described by the average power Ψ_l, the half-power bandwidth B_l and the central frequency ω_l, with respect to the lth eigenvalue of $\boldsymbol{Q}$. The white noise is contributed by the Poisson local dynamics. From the result demonstrated in [5], the influence of the white noise on a queueing system can be neglected.

If the traffic source is further assumed to be an $(M+1)$-state birth–death MMPP, which is a superposition of M independent and identically distributed (i.i.d.) two-state MMPPs with parameters (α, β, r_o) as shown in Fig. 1 , it would have all eigenvalues real and all bell-shaped functions zero-centered. Take a two-state MMPP for example, its time-domain traffic parameters described by (α, β, r_o) are shown in Fig. 2 *a*, and the PSD parameters characterised by $(\bar{\gamma}, B, \Psi)$ are shown in Fig. 2*b*, where $\bar{\gamma} = \beta r_o/(\alpha+\beta)$, $B = 2(\alpha+\beta)$ and $\Psi = \alpha\beta r_o/(\alpha+\beta)^2$. The PSD of the $(M+1)$-state birth–death MMPP can be obtained by composing PSDs of the M i.i.d. two-state MMPPs into a composite power spectrum which is further approximated by an impulse DC component and a single bell-shaped function with parameters

$$\bar{\gamma} = \frac{M\beta r_o}{\alpha+\beta} \tag{8}$$

$$B = 2(\alpha+\beta) \tag{9}$$

$$\Psi = \frac{M\alpha\beta r_o^2}{(\alpha+\beta)^2} \tag{10}$$

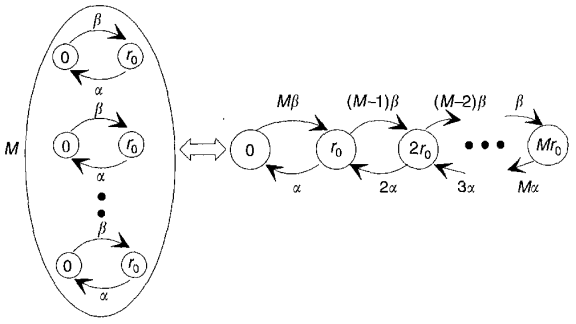

Fig. 1 *(M+1)-state birth–death MMPP model*

The composition algorithm for the two different power spectra is stated in the Appendix.

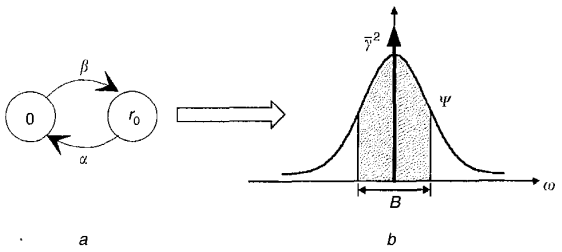

Fig. 2 *Time/frequency-domain parameters of the two-state MMPP*

Therefore, it can be concluded that a birth–death MMPP traffic source can be described by its PSD with power-spectrum parameters $(\bar{\gamma}, B, \Psi)$ including the DC component $(\bar{\gamma})$, the half-power bandwidth (B) and the average power (Ψ) of the bell-shaped function. These parameters can be obtained from the $(M+1)$-state MMPP parameters (α, β, r_o). The larger the mean input rate, the higher $\bar{\gamma}$ will be, the more correlated the input process is, the smaller B will be and the larger the input rate variance is, the higher Ψ will be. Moreover, the PSD parameters of the input process possess the additive property, which does not exist in the time-domain traffic parameters.

When a new call request provides its time-domain traffic parameters such as peak bit rate (R_P), mean bit rate (R_M) and average peak bit rate duration (T_D) during the call establishment phase, the modelled $(M+1)$-state birth–death MMPP process with parameters (α, β, r_o) can be obtained from these traffic parameters (R_P, R_M, T_D) by

$$\alpha = \frac{1}{MT_D} \tag{11}$$

$$\beta = \frac{R_M}{MT_D(R_P - R_M)} \tag{12}$$

$$r_o = \frac{R_P}{M} \tag{13}$$

The power-spectrum parameters $(\bar{\gamma}, B, \Psi)$ of the input traffic of the new call can then be converted from the $(M+1)$-state birth–death MMPP parameters (α, β, r_o) by (8)–(10).

3 PSD-based neural-net connection admission controller

Fig. 3 shows the functional block diagram of the PSD-based neural-net connection admission controller. It mainly contains a PNCAC controller, a time/frequency parameters converter, a data rate register, a PSD parameter register, a data rate composer and a power spectrum composer. Input traffic is assumed to be classified into two types. Type-1 traffic is the real-time traffic such as voice and video, and type-2 traffic is the non-real-time traffic such as data.

As the new call request for type-1 traffic claims its traffic parameters, R_P, R_M and T_D, in the call establishment phase, the time/frequency parameter converter transforms the (R_M, R_P, T_D) in the time domain into $(\bar{\gamma}, B, \Psi)$ in the frequency domain. The PSD parameter register keeps the record of the power-spectrum parameters $(\bar{\gamma}_E, B_E, \Psi_E)$ of the total existing type-1 connections, where $\bar{\gamma}_E$ is the total average input rate, B_E is the total half-power bandwidth and Ψ_E is the total average power. The two sets of parameters $(\bar{\gamma}, B, \Psi)$ and $(\bar{\gamma}_E, B_E, \Psi_E)$ are added to form a new set of parameters $(\bar{\gamma}_T, B_T, \Psi_T)$ through the power spectrum composer which performs the power spectrum composition and approximation functions mentioned in the Appendix. If the new call request belongs to type-2 data traffic, it claims the data rate Γ as the traffic parameters in the call establishment phase. The data rate register records the overall data rate Γ_E of the existing type-2 connections, and the data rate composer adds these two data rates, Γ and Γ_E, to form a new parameter Γ_T. The set of PSD parameters $(\bar{\gamma}_T, B_T, \Psi_T)$ accompanied by the data rate Γ_T is then fed into the *PNCAC controller* as the input variables. As shown in Fig. 4 , the PNCAC controller is a multilayer feedforward neural network [10, 12], which possesses capabilities of approximation to a perfect connection acceptance decision function. A back-propagation learning algorithm [13] is used here to train the neural network. The PNCAC controller will then decide whether to accept or reject this connection request using the neural network and feed the decision output (Y) back to the source.

If the decision is to accept the new type-1 call, the PSD parameter register will be triggered to update the stored power-spectrum parameters $(\bar{\gamma}_E, B_E, \Psi_E)$ to be $(\bar{\gamma}_T, B_T, \Psi_T)$. Similarly, so does the type-2 data rate register if a type-2 call is accepted. If the decision is to reject the new call, no updating procedure is needed. Notice that $(\bar{\gamma}, B, \Psi)$

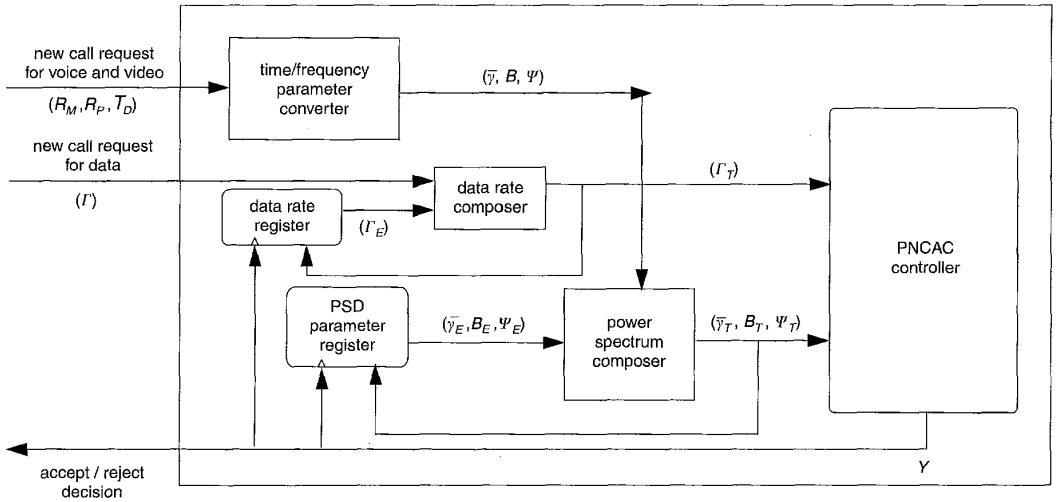

Fig. 3 *Functional block diagram of the PSD-based neural-net connection admission controller*

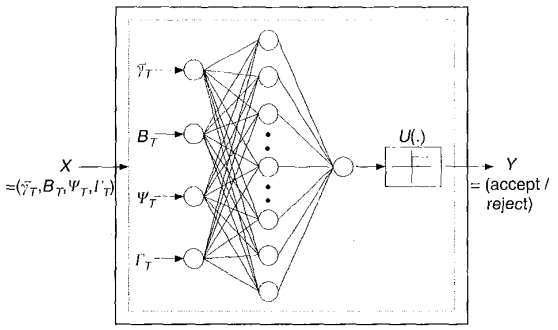

Fig. 4 *Basic structure of the PNCAC controller*

or Γ should be subtracted from $(\bar{\gamma}_E, B_E, \Psi_E)$ or Γ_E when a type-1 or type-2 call is disconnected, respectively, which is not shown here.

The implementation of the proposed PNCAC takes about 200 lines of C codes, in which 370 multiplication and 310 addition operations are included. The computation time to make an admission decision would be no more than 500 μs under general purpose CPU such as Intel Pentium-II or above. Therefore, the PNCAC would be feasible in real implementation for high-speed multimedia networks. If special purpose CPU or DSP processors with pipeline architecture or optimised computation capabilities are adopted, less time should be taken to respond to a call request. Also, the compiled machine (execution) codes for Intel CPU occupy about 20 kbyte. The proposed PNCAC scheme can even be downloaded to the embedded systems (platforms).

4 Simulation results and discussions

Here we assume that the call admission controller is designed in an ATM switch/router in multimedia networks, and input messages are segmented into fixed-length ATM cells. Two separate buffers with buffer size K1 and K2 are for type-1 and type-2 traffic, respectively. One buffer space can accommodate one ATM cell. When the buffer is full, new coming cells are blocked and lost. The service discipline for type-1 and type-2 traffic is that the system initially allocates equal capacity for both types, and the remaining capacity of one type of traffic can be used by the other type of traffic.

In the simulations, the buffer sizes K1 and K2 are all set to be 100 cells; the system capacity is assumed to be 150 Mbit/s. Different QoS requirements for these two types of traffic are defined: the required cell loss probability is set to be 10^{-5} for type-1 traffic and 10^{-6} for type-2 traffic. The voice sources are modelled by a two-state on-off Markov chain (MMPP); the video sources are modelled by a modified Markov process addressed in [11], where the numbers of video interframes and intraframes are assumed to have five states, and the data sources are modelled by a Poisson process. The traffic parameters for voice and video sources are shown in Table 1, and the mean rate for data sources is 1 Mbit/s. The call arrival rate for voice is 15.4 calls/s with mean holding time of one minute, the call arrival rate for video is 0.082 calls/s with mean holding time of five minutes, and the call arrival rate for data is 3.2 calls/s with mean holding time of 20 s. For all traffic types, the call arrival processes are assumed to be independently Poisson distributed, and the mean holding time is assumed to be exponentially distributed. Note that in the transformation of the three input time-domain parameters (R_M, R_P, T_D) into PSD parameters $(\bar{\gamma}, B, \Psi)$, both voice and video sources are assumed to be two-state birth–death MMPP.

Table 1: Traffic source parameters

Traffic parameters	Peak rate	Mean rate	Peak rate duration
Voice	64.0 kbit/s	27.6 kbit/s	1.366 s
Video	5.7 kbit/s	1.9 Mbit/s	0.033 s
Data	–	1.0 Mbit/s	–

The neural networks adopted by the PNCAC is a three-layered fully-connected feedforward neural network with 50 hidden nodes, as the one used by Hiramatsu's NNCAC which has 30 hidden nodes. It uses 683 and 280 training data and takes about 221467 and 199501 iterations to thoroughly train the PNCAC and Hiramatsu's NNCAC, respectively.

Fig. 5 shows the cell loss ratio of type-1 and type-2 traffic, and the system utilisation in Figs. 5*a*, *b* and *c* respectively, for the three approaches, where the characteristics of traffic source in simulation are exactly the same as the ones used in the training data generation phase. We can find that, after the neural networks have been well trained, both Hiramatsu's NNCAC and PNCAC have larger cell loss ratio than ECCAC, but still guarantee QoS requirements, while Hiramatsu's NNCAC and PNCAC can improve significantly the system utilisation over the conventional ECCAC by about 24.4% and 23.8%, respectively. Note that this utilisation is obtained by averaging those values between 10^9 and 2×10^9 slot times. This is because of the learning and adaptive capability of neural networks. Also, Hiramatsu's NNCAC has slightly better system utilisation than PNCAC by about 0.6%, as Hinamatsu's NNCAC adopts the connection number of each traffic characteristic as the input to decide whether a call request is accepted or not, and the traffic characteristics in simulations are exactly the same as the ones used in the training data generation phase for Hiramatsu's NNCAC.

We further consider two simulation examples when the neural networks were well trained according to the traffic characteristics illustrated in Table 1, but the system receives heavier and lighter traffic sources with parameters in Tables 2 and 3, respectively.

Fig. 6 shows the cell loss ratio of type-1 and type-2 traffic, and the system utilisation, for the heavier traffic source, in Figs. 6*a*, *b* and *c*, respectively. It can be seen that the cell loss ratio of Hiramatsu's NNCAC, denoted by the dashed line, seriously violates the QoS requirements, in both type-1 and type-2 traffic, although the utilisation of Hiramatsu's NNCAC is the highest one and approaches 100%. However, the proposed PNCAC and ECCAC can still fulfil the QoS requirements, and the system utilisations of PNCAC and ECCAC are 85.8% and 77.7%, respectively.

Fig. 7 shows the cell loss ratios of type-1 and type-2 traffic, and the system utilisation, for the lighter traffic source, in Figs. 7*a*, *b*, and *c*, respectively. It can be seen that all the three CAC schemes have zero cell loss ratios and guarantee the required QoS but obtain low system utilisations, compared to those of the normal case shown in Fig. 5. Hiramatsu's NNCAC suffers more degradation and turns out to have the worst system utilisation.

From these two simulation examples, it can be concluded that Hiramatsu's NNCAC has worse adaptivity and flexibility than PNCAC and ECCAC. This is because the connection number of each traffic type adopted by

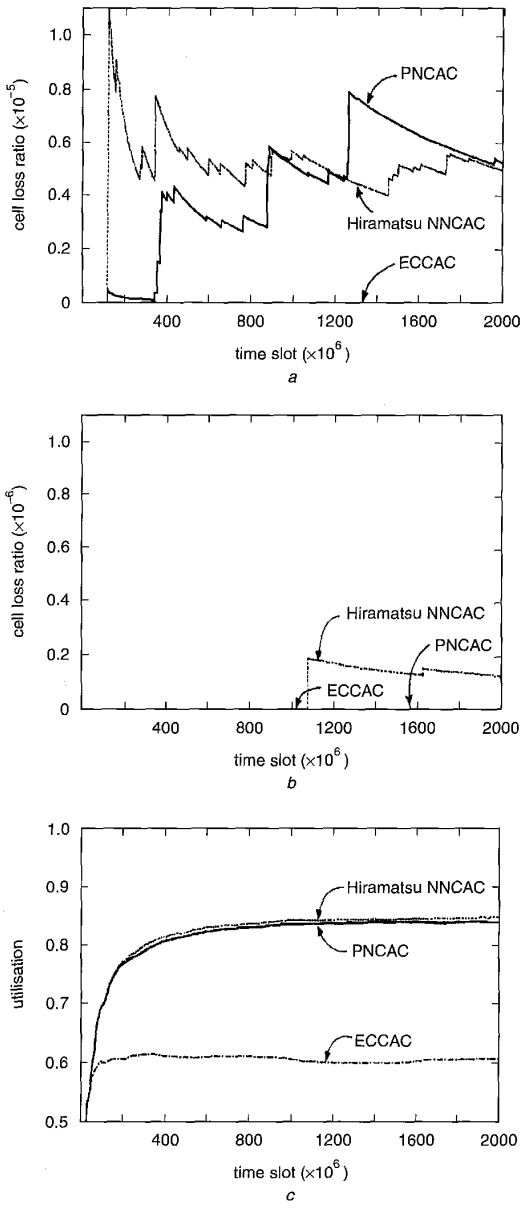

Fig. 5 *Cell loss ratios and system utilisation*
a Type-1 cell loss ratio (CLR)
b Type-2 cell loss ratio (CLR)
c System utilisation of the ECCAC, Hiramatsu's NNCAC, and PNCAC

Table 2: Heavier traffic source parameters

Traffic parameters	Peak rate	Mean rate	Peak rate duration
Voice	64.0 kbit/s	40.958 kbit/s	1.742 s
Video	11.4 Mbit/s	3.8 Mbit/s	0.033 s
Data	—	1.5 Mbit/s	—

Table 3: Lighter traffic source parameters

Traffic parameters	Peak rate	Mean rate	Peak rate duration
Voice	64.0 kbit/s	23.042 kbit/s	0.98 s
Video	2.85 Mbit/s	0.95 Mbit/s	0.033 s
Data	—	0.5 Mbit/s	—

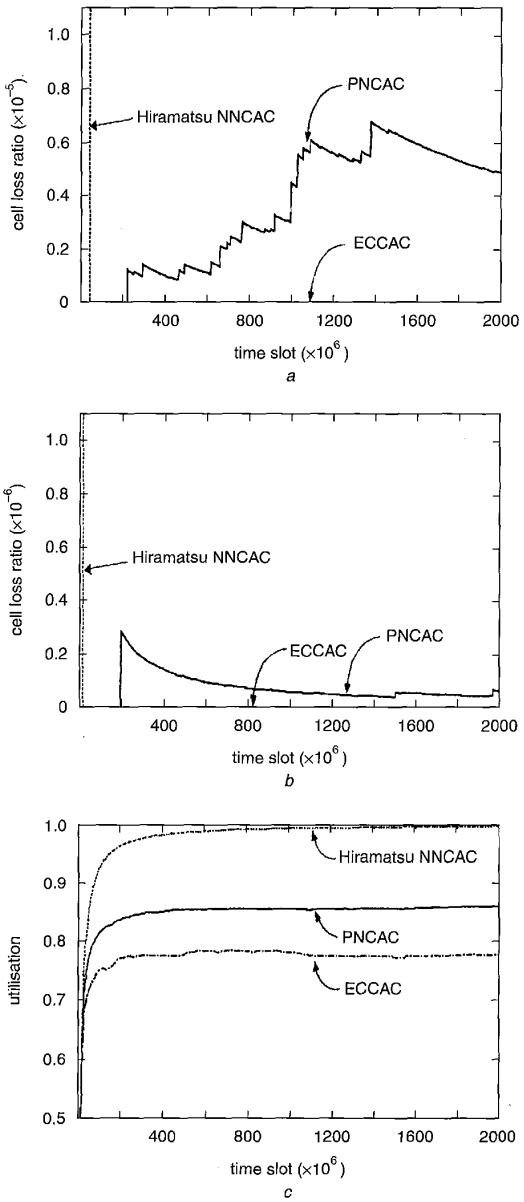

Fig. 6 *Cell loss ratios and system utilisation for heavier traffic sources*
a Type-1 cell loss ratio (CLR)
b Type-2 cell loss ratio (CLR)
c System utilisation of the ECCAC, Hiramatsu's NNCAC, and PNCAC with heavier traffic sources

Hiramatsu's NNCAC could apply only when the traffic characteristics of traffic sources fed into the operational system are the same as the ones in the training phase. However, this is usually impossible in real practice. As traffic characteristics of sources change, the neural network should learn to adapt to the variation in sources by online training, and moreover, the structure of the neural network should be modified to have proper inputs by a node-

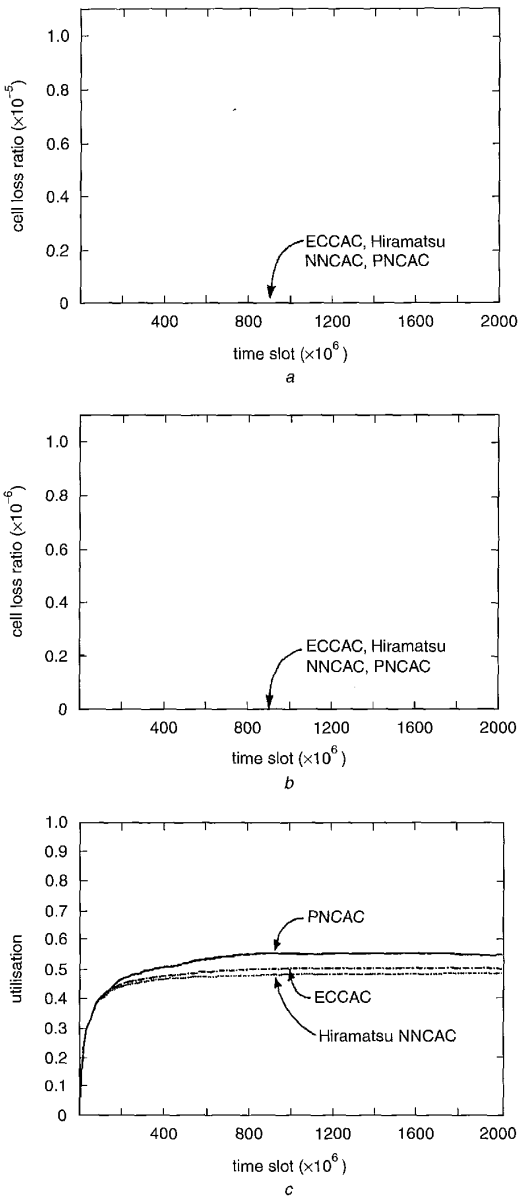

Fig. 7 *Cell loss ratios and system utilisation for lighter traffic sources*
a Type-1 cell loss ratio (CLR)
b Type-2 cell loss ratio (CLR)
c System utilisation of the ECCAC, Hiramatsu's NNCAC, and PNCAC with lighter traffic sources

growing or node-pruning learning process, if necessary. This would make Hiramatsu's NNCAC infeasible. Because both ECCAC and PNCAC depend on traffic characteristic parameters which can react to the variation in traffic characteristics, these two schemes can adapt to traffic properly without any other modifications or retraining and still perform the CAC decision well. It is also because the transformed equivalent capacity for ECCAC and the PSD parameters for PNCAC are both unified metrics corresponding to traffic characteristics of all different sources and possess the additive property, while the connection number adopted by Hiramatsu's NNCAC as the input variables for neural networks could not be summed for different traffic types.

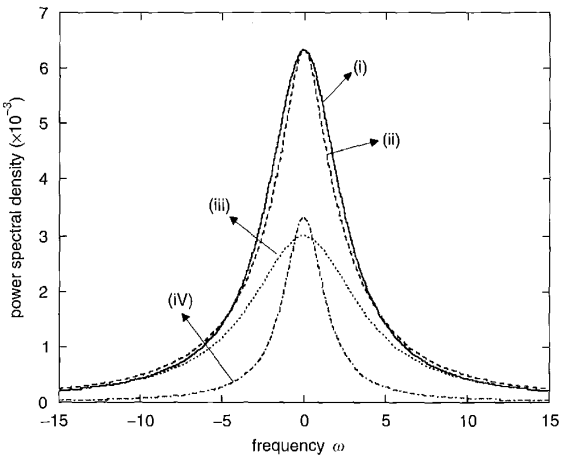

Fig. 8 *Approximated bell-shaped function*
(i) Approximated bell-shaped function $b(\omega)$
(ii) Composite power spectrum $b_1(\omega)+b_2(\omega)$
(iii) Bell-shaped function $b_1(\omega)$
(iv) Bell-shaped function $b_2(\omega)$

In addition, the proposed PNCAC has better performance than ECCAC. Both PNCAC and ECCAC depend on traffic characteristic parameters. However, PNCAC transforms the three time-domain traffic characteristic parameters into the corresponding three PSD-domain parameters, while ECCAC converts the same time-domain parameters to a single equivalent capacity. Although the equivalent capacity is also additive, the proposed PNCAC adopts the three PSD parameters as the inputs of neural networks to perform the CAC decision, which could capture more traffic characteristics and less composition approximation error than the single equivalent capacity. The self-learning capability of neural network also makes the PNCAC more adaptive to the traffic.

5 Concluding remarks

In this paper, we propose a power-spectrum-based neural-net connection admission control (PNCAC) scheme for multimedia networks. The PNCAC method adopts the converted power-spectrum parameters of traffic sources to represent its traffic characteristics and uses a neural network to implement the connection admission control. The frequency-domain power-spectrum parameters of traffic sources possess the additive property and can capture the correlation and burstiness behaviour more than the time-domain parameters such as peak rate, mean rate and peak rate duration. The neural network has learning/adapting capabilities so that the boundary of the decision hyperplane for the connection admission control can be adjusted optimally and dynamically. We demonstrate results whenever the input voice and video traffic sources are modelled by MMPP and modified MMPP, respectively, and the data traffic sources are modelled by a Poisson process. Simulation results show that the proposed PNCAC enhances significantly the system utilisation while fulfilling QoS requirements. Not only is it superior to the conventional equivalent capacity CAC scheme (ECCAC), but it also obtains more flexibility and robustness than Hiramatsu's NNCAC.

6 Acknowledgments

This work was supported by the National Science Council, Taiwan, under contract numbers 88-2213-E-009-088 and 89-2213-E-009-105 and by Lee and MTI Center for Networking Research at National Chiao Tung University, Taiwan.

7 References

1 ITU-T Recommendation 1.371: 'Traffic control and congestion control in B-ISDN'. Geneva, May 1996
2 GUERIN, R., AHMADI, H., and NAGHSHINEH, M.: 'Equivalent capacity and its application to bandwidth allocation in high-speed networks', *IEEE J. Sel. Areas Commun.*, 1991, **9**, (7), pp. 968–981
3 ELWALID, A.I., and MITRA, D.: 'Effective bandwidth of general Markovian traffic sources and admission control of high speed networks', *IEEE/ACM Trans. Netw.*, 1993, **1**, (3), pp. 329–343
4 SAITO, H.: 'Call admission control in an ATM network using upper bound of cell loss probability', *IEEE Trans. Commun.*, 1992, **40**, (9), pp. 1512–1521
5 LI, S.Q., and HWANG, C.L.: 'Queue response to input correlation functions: continuous spectral analysis', *IEEE/ACM Trans. Netw.*, 1993, **1**, (6), pp. 678–692
6 SHENG, H.D., and LI, S.Q.: 'Spectral analysis of packet loss rate at a statistical multiplexer for multimedia services', *IEEE/ACM Trans. Netw.*, 1994, **2**, (1), pp. 53–65
7 THERRIEN, C.W.: 'Discrete random signals and statistical signal processing' (Prentice–Hall, New Jersey, 1992)
8 CHANG, C.J., LIN, C.H., GUAN, D.S., and CHENG, R.G.: 'Design of a power-spectrum-based ATM connection admission control for multimedia communications', *IEEE Trans. Ind. Electron.*, 1998, **45**, (1), pp. 52–59
9 HIRAMATSU, A.: 'ATM communications network control by neural networks', *IEEE Trans. Neural Netw.*, 1990, **1**, (1), pp. 122–130
10 CHENG, R.G., and CHANG, C.J.: 'Neural-network connection admission control for ATM networks', *IEE Proc., Commun.*, 1997, **144**, (2), pp. 93–98
11 CHENG, R.G., CHANG, C.J., and LIN, L.F.: 'A QoS provisioning neural fuzzy connection admission controller for multimedia high-speed networks', *IEEE/ACM Trans. Netw.*, 1999, **7**, (1), pp. 111–121
12 LIN, C.T., and LEE, C.S.G.: 'Neural fuzzy sytems: a neuro-fuzzy synergism to intelligent systems' (Prentice–Hall, Singapore, 1996)
13 RUMELHART, D.E., HINTON, G.E., and WILLIAMS, R.J.: 'Learning internal representation by error propagation' in 'Parallel distributed processing: Explorations in the microstructure of cognition' (MIT Press, Cambridge, MA, USA, 1986), vol. 1, Chap. 8

8 Appendix: Composition algorithm for power spectra

Assume that $b_1(\omega)$ and $b_2(\omega)$ are two bell-shaped functions corresponding to zero-centred PSDs with parameters $(\bar{\gamma}_1, B_1, \Psi_1)$ and $(\bar{\gamma}_2, B_2, \Psi_2)$, as shown in Fig. 8 , and that $b(\omega)$ is the approximated bell-shaped function corresponding to the composite power spectrum with parameters $(\bar{\gamma}, B, \Psi)$. To compose the two zero-centred PSDs, we add the two DC components and the two bell-shaped functions directly. We then approximate $b_1(\omega)+b_2(\omega)$ to be $b(\omega)$. In the approximation, we set $\Psi=\Psi_1+\Psi_2$, and $b(\omega)=b_1(\omega)+b_2(\omega)$ at $\omega=0$. Therefore, $(\bar{\gamma}, B, \Psi)$ of the approximated power spectrum are given by

$$\bar{\gamma} = \bar{\gamma}_1 + \bar{\gamma}_2 \tag{14}$$

$$B = \frac{(\Psi_1 + \Psi_2)B_1B_2}{\Psi_1B_2 + \Psi_2B_1} \tag{15}$$

$$\Psi = \Psi_1 + \Psi_2 \tag{16}$$

Note that the approximated bell-shaped function contains more low-frequency components than $b_1(\omega)+b_2(\omega)$.